

LoFT-LLM: Low-Frequency Time-Series Forecasting with Large Language Models

Jiacheng You

School of Computer Science and Technology, Harbin Institute of Technology (Shenzhen)
Shenzhen, China
jiachengyou2hit@gmail.com

Zhongxuan Wu

School of Computer Science and Technology, Harbin Institute of Technology (Shenzhen)
Shenzhen, China
wuzhongxuan7@outlook.com

Pengjie Wang

Unaffiliated
Beijing, China
wangpengjie0421@163.com

Jingcheng Yang

Unaffiliated
Beijing, China
jingchengyang95@gmail.com

Yuhang Xie

The Chinese University of Hong Kong
Hong Kong, China
yuhangxie@link.cuhk.edu.hk

Xiucheng Li

School of Computer Science and Technology, Harbin Institute of Technology (Shenzhen)
Shenzhen, China
lixiucheng@hit.edu.cn

Feng Li

Unaffiliated
Beijing, China
lifeng_passion@163.com

Jian Xu

Unaffiliated
Beijing, China
jian.xu.mail@qq.com

Bo Zheng

Unaffiliated
Beijing, China
bo.zheng@gmail.com

Xinyang Chen*

School of Computer Science and Technology, Harbin Institute of Technology (Shenzhen)
Shenzhen, China
chenxinyang95@gmail.com

through structured natural language prompts. Extensive experiments on financial and energy datasets demonstrate that LoFT-LLM significantly outperforms strong baselines under both full-data and few-shot regimes, delivering superior accuracy, robustness, and interpretability.

CCS Concepts

- Computing methodologies → Neural networks; Natural language processing;
- Information systems → Data mining.

Keywords

Time Series Forecasting; Low-Frequency Learning; Few Shot; Large Language Models

ACM Reference Format:

Jiacheng You, Jingcheng Yang, Yuhang Xie, Zhongxuan Wu, Xiucheng Li, Feng Li, Pengjie Wang, Jian Xu, Bo Zheng, and Xinyang Chen. 2026. LoFT-LLM: Low-Frequency Time-Series Forecasting with Large Language Models. In *Proceedings of the 32nd ACM SIGKDD Conference on Knowledge Discovery and Data Mining V.1 (KDD '26)*, August 09–13, 2026, Jeju Island, Republic of Korea. ACM, New York, NY, USA, 16 pages. <https://doi.org/10.1145/3770854.3780245>

*Corresponding author.



This work is licensed under a Creative Commons Attribution 4.0 International License.
KDD '26, Jeju Island, Republic of Korea
© 2026 Copyright held by the owner/author(s).
ACM ISBN 979-8-4007-2258-5/2026/08
<https://doi.org/10.1145/3770854.3780245>

1 Introduction

Time-series forecasting underpins a wide spectrum of high-stakes applications, including energy demand planning [21, 48], meteorology [6, 8], and financial risk management [2, 14]. Modern deep networks achieve remarkable accuracy when tens of thousands of examples are available, yet in practice such volumes are costly, proprietary, or simply unattainable, making data scarcity a fundamental challenge in many practical settings.

Data scarcity amplifies two fundamental challenges in time series forecasting. First, limited data often contain dominant high-frequency noise, which undermines the generalization of deep forecasting models by masking underlying patterns [29, 41]. This noise makes it difficult for models to identify meaningful low-frequency dependencies that are critical for capturing long-term trends and global cycles [44]. While deep models have shown promise in learning complex temporal patterns, conventional training strategies often struggle to emphasize low-frequency signals, a weakness that is amplified in real-world, data-scarce settings where these dependencies are harder to recover. Second, real-world log data contain a rich mix of heterogeneous signals. The primary forecast target, for example a fund’s daily trades, is recorded alongside numerous auxiliary variables, ranging from click-through rates to macroeconomic indicators. Most existing methods simply normalize these disparate fields into numeric vectors and fit model parameters accordingly [18, 36]. This pipeline strips away valuable context, such as page views, market dynamics, interest-rate regimes, and more, so the model cannot tap into domain knowledge that could guide learning. The deficiency is magnified in few-shot settings: without a mechanism to inject semantics, the model underutilizes high-level priors, ultimately harming both forecasting accuracy and interpretability.

Recent methodological insights offer promising directions. On the optimization side, gradient-based networks exhibit a spectral bias, learning low-frequency components faster, and with fewer samples than high-frequency ones [26, 41]. Explicitly isolating and supervising these slow trends can thus provide a stable foundation in few-shot regimes, while treating the residual high-frequency content as a separate modelling task prevents the main network from overfitting to noise.

On the representation side, large language models (LLMs) have demonstrated an ability to ingest heterogeneous cues, such as numbers, categorical attributes, and textual rules, within a single prompt and to reason over their interactions [47]. This capability enables the LLM to serve as a semantic calibrator: when frequency-specific predictions and domain descriptors are embedded as prompt elements, the model can inject prior knowledge and correct systematic biases that purely numerical modules overlook. Beyond their representational power, LLMs also excel in in-context learning and lightweight fine-tuning [22], making them highly effective at integrating domain and context information in data-scarce settings [3, 15]. These strengths motivate the exploration of LLMs for few-shot time-series forecasting, where training samples are limited yet auxiliary business knowledge abounds.

Building on these insights, we first propose a frequency-aware supervision strategy that filters out high-frequency noise within the prediction window and directly trains models to capture dominant low-frequency components. To better align predictions with true

frequency structures, we adopt Frequency Alignment Loss (FALoss) inspired by FreDF [32], which minimizes the absolute distance between the corresponding Fourier coefficients of predictions and ground truth. Since real-world time series typically exhibit strong low-frequency trends that appear as distinct peaks in the frequency spectrum, this objective inherently encourages accurate modeling of long-term dependencies.

Finally, we present LoFT-LLM (Low-Frequency Time-series forecasting with Large Language Models), a three-phase architecture designed for data-scarce environments.

Phase 1 (Low-frequency pre-training). We design a Patch Low-Frequency forecasting Module (PLFM) that incorporates FALoss and directly learns low-frequency knowledge from the perspective of the frequency domain, demonstrating excellent capabilities in discovering low-frequency dependencies.

Phase 2 (Residual learning). With the PLFM weights frozen, a lightweight backbone takes high-pass-filtered inputs and models the remaining high-frequency dynamics, cleanly separating noise from trend.

Phase 3 (LLM fine-tuning). A large language model is then parameter-efficiently fine-tuned using prompts that package (i) the PLFM trend, (ii) the high-frequency residual, and (iii) auxiliary textual or categorical context. Acting as a semantic calibrator, the LLM reconciles these ingredients, injecting domain knowledge and correcting systematic biases to yield a refined forecast.

At inference time, the frozen modules, namely PLFM, the residual backbone, and the fine-tuned LLM, form a compact predictor that delivers high accuracy without further adaptation, making LoFT-LLM well-suited to real-world, data-sparse deployments.

Our contributions are summarized as follows:

- We propose a frequency-aware learning strategy via the Patch Low-Frequency forecasting Module (PLFM), which captures dominant trends through localized spectral modeling. Frequency Alignment Loss (FALoss) further stabilizes training by encouraging spectral consistency, enhancing robustness in data-scarce regimes.
- We present LoFT-LLM: a three-phase, frequency-aware pipeline. PLFM is combined with a lightweight residual learner for high-frequency dynamics and an LLM fine-tuned in a parameter-efficient manner that ingests PLFM trends, residual spikes, and auxiliary context through a frequency-tagged prompt. The LLM acts as a semantic calibrator, injecting domain knowledge and correcting systematic biases without costly retraining.
- We conduct comprehensive experiments on two real-world datasets, and our method outperforms the current state-of-the-art forecasting methods on all datasets.

2 Related Work

2.1 Time Series Forecasting

Deep learning models have become the dominant paradigm in time series forecasting. Early RNN-based models, such as LSTNet [16] and DeepAR [27], leverage sequence-to-sequence structures to capture temporal dependencies. Transformer-based approaches later emerged as powerful alternatives, offering superior scalability and

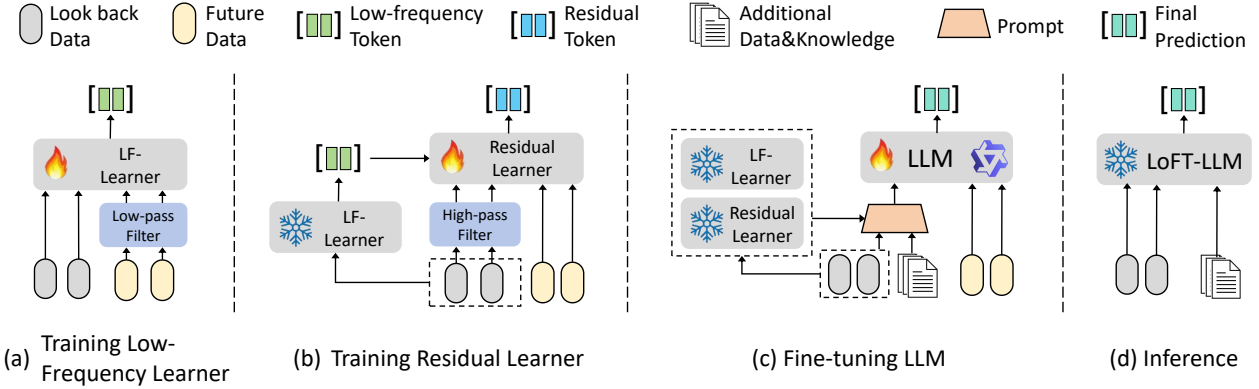


Figure 1: LoFT-LLM training and inference pipeline. (a) Training the low-frequency learner (PLFM) using filtered ground truth. (b) Training the residual learner with PLFM fixed. (c) Fine-tuning the LLM using prompt constructed from both learners and auxiliary information. (d) Inference combines all modules to generate final predictions.

the ability to model long-range correlations. Informer [49] accelerates attention computation via self-attention distillation; Autoformer [37] incorporates time series decomposition; Non-stationary Transformer [20] adapts attention mechanisms to capture non-stationary patterns; PatchTST [24] introduces channel-independent patch modeling; and iTransformer [18] reorders the architecture to enhance multivariate representation. Besides, lightweight MLP-based models [5, 7, 45, 46] also show excellent performance for forecasting tasks. Recently, several forecasting models have focused on learning the knowledge from the frequency domain to boost predicting performance. Specifically, FEDformer [51] and FiLM [50] incorporate frequency information as supplementary features to enhance the model’s capability to capture long-term periodic patterns. FrTS [42] introduces frequency domain-based MLP to learn both channel-wise and time-wise dependencies. FITS [40] discards the high-frequency components to reduce the parameter scale, making it easy to deploy in edge devices. FrDF [32] introduces a Fourier-based discrepancy function to align the spectral distributions of predictions and ground truth, offering a principled frequency-level supervision strategy.

However, these advanced models still adhere to the conventional training paradigm, leveraging temporal loss functions and supervised signals, which can be easily influenced by high-frequency data and have limitations in low-frequency learning. Moreover, they often lack mechanisms to incorporate external or domain-specific information, which hinders performance on datasets where auxiliary variables play a crucial role in accurate forecasting.

2.2 Large Language Models

The rapid progress of large language models (LLMs) has sparked growing interest in their application to time series forecasting, especially under few-shot and heterogeneous data scenarios. GPT4TS [52] adapts GPT2 to model pure numerical sequences, demonstrating the feasibility of autoregressive forecasting using LLMs. LLM4TS [4] proposes a two-phase fine-tuning pipeline that first aligns LLMs with structural patterns in time series, then applies

forecasting-specific training. Time-LLM [13] reformulates numerical inputs into contextual embeddings and leverages prompt-as-prefix generation for downstream prediction. AutoTimes [19] maps multivariate time series into the token embedding space of decoder-only LLMs, enabling zero-shot or few-shot inference without gradient updates. To enhance scalability and external knowledge integration, TimeMoE [28] employs a sparse mixture-of-experts architecture to handle diverse forecasting contexts, though its performance degrades in low-resource settings due to routing inefficiencies. News2Forecast [34] introduces reflective LLM agents that incorporate social news signals to enrich time series forecasting. TimeKD [17] uses privileged cross-modal teachers to guide student LLMs trained with limited input.

While LLMs have recently been applied to time series forecasting, most fail to incorporate core temporal modeling techniques such as frequency decomposition or residual learning. They often treat forecasting as generic sequence generation and rely heavily on pretraining, limiting effectiveness in few-shot settings. In contrast, our method integrates frequency-aware predictions with structured prompts to enable LLM-based semantic calibration, improving robustness and interpretability under data scarcity.

2.3 Frequency Modeling in Deep Learning.

Frequency modeling can provide a clear representation from the perspective of the frequency domain and has been widely applied in the field of computer vision (CV) [11, 33, 38], where low-pass and high-pass filtering are commonly used to model high-frequency structural knowledge and low-level semantic information respectively. Compared to the high-frequency counterparts in images that often exhibit clear structural features, the high-frequency components prevalent in time series data often include a large amount of noise and anomalies, severely affecting low-frequency learning. Different from frequency modeling in CV, our proposed frequency learning module is designed to separate the high-frequency components in the prediction window, facilitating effective low-frequency learning and alleviating limitations of traditional training paradigms.

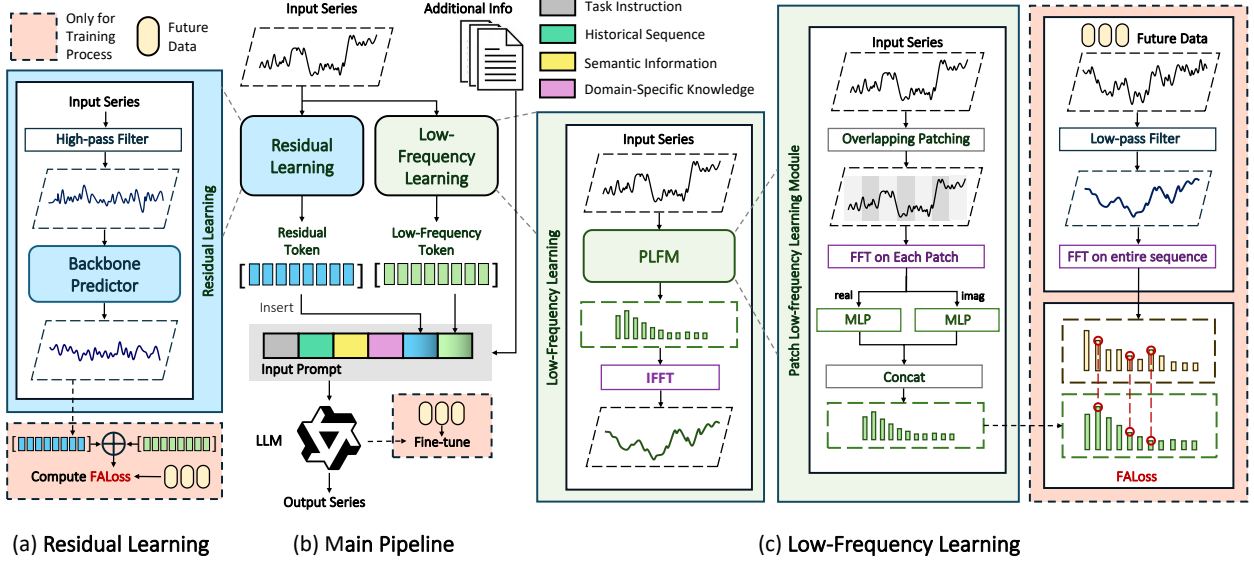


Figure 2: Overall architecture of LoFT-LLM. (a) Structure of the residual learner, consisting primarily of a configurable backbone predictor. (b) The main pipeline of the LoFT-LLM. (c) Internal architecture and PLFM. Components highlighted with red dashed boxes are used only during training.

3 Method

Problem Formulation. Given a historical multivariate time series observations $\mathbf{X} = [\mathbf{x}^{(0)}, \mathbf{x}^{(1)}, \dots, \mathbf{x}^{(C-1)}] \in \mathbb{R}^{H \times C}$ sampled at H timestamps with C channels. The forecasting formulation aims to predict the next L (prediction window length) time step observations $\mathbf{Y} = [\mathbf{y}^{(0)}, \mathbf{y}^{(1)}, \dots, \mathbf{y}^{(C-1)}] \in \mathbb{R}^{L \times C}$. Note that $\mathbf{Y}_{t,:}$ (the t -th row of \mathbf{Y}) is simply an alias of $\mathbf{X}_{t+H,:}$ with $\mathbf{Y}_{t,:} = \mathbf{X}_{t+H,:}$ for $t = 0, \dots, L-1$. In addition to historical observations, we assume access to auxiliary information $\mathbf{A} \in \mathbb{R}^{(H+L) \times D}$, which includes contextual features associated with both past and future time steps. The forecasting task is to learn a model parameterized by θ : $f_\theta: \mathbf{X}^{H \times C}, \mathbf{A}^{(H+L) \times D} \mapsto \mathbf{Y}^{L \times C}$.

Overall Idea. We propose a frequency-aware and semantically guided framework for time series forecasting. As shown in Figure 1, the model follows a three-stage training process: (a) a Patch Low-Frequency forecasting Module (PLFM) learns dominant trend components from filtered targets to form a stable prediction backbone; (b) a residual learner fits high-frequency variations as corrective signals; and (c) a large language model (LLM) is fine-tuned via prompt-based supervision to semantically calibrate the combined outputs using auxiliary context. This design prioritizes low-frequency structure while leveraging high-frequency and semantic cues for refinement, resulting in robust and interpretable forecasts in few-shot settings.

3.1 Frequency Alignment Loss

The mainstream loss functions in time series forecasting are temporal domain-based MSE and MAE, which leverage point-wise alignment methods and pay great attention to the alignment with high-frequency fluctuations and noise, making it difficult to discover clear low-frequency dependencies. To address this issue, we

follow the approach proposed in FreDF [32] and design FALoss to better align with low-frequency components.

Specifically, given prediction window $\mathbf{Y}^{L \times C}$ and model output $\mathbf{Y}^o \in \mathbb{R}^{L \times C}$, FALoss first employs Discrete Fourier Transform (DFT) to convert \mathbf{Y} and \mathbf{Y}^o into frequency domain by treating each channel independently. For convenience, we focus on one particular channel and drop the superscript to keep the notation uncluttered when the context is clear. The DFT transforms \mathbf{y} and \mathbf{y}^o as follows:

$$\hat{y}_k = \sum_{n=0}^{L-1} y_n e^{-2\pi i \frac{n}{N} k}, \quad k = 0, 1, \dots, L-1, \quad (1)$$

where \hat{y}_k denotes the k -th Fourier coefficient of the signal \mathbf{y} . Let $\hat{\mathbf{y}} \triangleq [\hat{y}_0, \dots, \hat{y}_{L-1}]$, then we can obtain $\hat{\mathbf{Y}} \triangleq [\hat{\mathbf{y}}^{(0)}, \hat{\mathbf{y}}^{(1)}, \dots, \hat{\mathbf{y}}^{(C-1)}]$ by transforming each channel identically. Let \mathbf{y}^o denotes the prediction of \mathbf{y} , we can acquire $\hat{\mathbf{Y}}^o \triangleq [\hat{\mathbf{y}}^{o,(0)}, \hat{\mathbf{y}}^{o,(1)}, \dots, \hat{\mathbf{y}}^{o,(C-1)}]$ in an analogous manner. Given \mathbf{Y} and \mathbf{Y}^o , the FALoss is defined to be the mean absolute error of their Fourier coefficients as follows:

$$\mathcal{L}_{\text{FA}}(\mathbf{Y}, \mathbf{Y}^o) = \frac{1}{L \times C} \|\hat{\mathbf{Y}} - \hat{\mathbf{Y}}^o\|_1. \quad (2)$$

3.2 Patch Low-Frequency Forecasting Module

The current mainstream time series forecasting paradigms utilize temporal prediction windows as supervised signals, which contain a significant amount of high-frequency data. These high-frequency components are often associated with oscillations, anomalies, and noise, posing serious challenges to the low-frequency modeling and generalization of deep forecasters. Besides, considering that low-frequency components in time series that oscillate less frequently and have longer wavelengths, generally appear as distinct peaks in

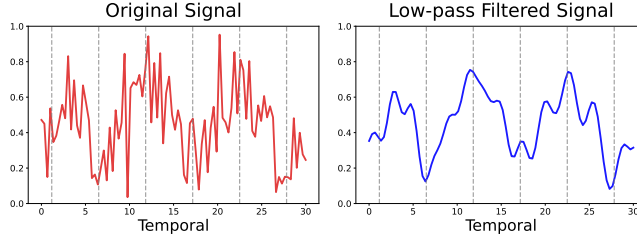


Figure 3: Visualization of noisy time series and its low-pass filtered counterpart. The filtered signal highlights dominant low-frequency trends, which are used as supervision targets in our frequency-aware learning strategy.

the frequency spectrum and show strong global dependencies, making it suitable for frequency domain-based forecasters to discover the global and low-frequency patterns.

To alleviate the influence of high-frequency parts and empower forecasting models with better low-frequency learning capabilities, we filter out high-frequency parts in the prediction window and introduce Patch Low-Frequency forecasting Module (PLFM) to use the frequency patch spectra as supervised signals, directly discovering clear low-frequency dependencies from the frequency domain. Rather than applying FFT over the entire sequence, which may obscure temporal locality, PLFM adopts a localized spectral modeling strategy inspired by the Short-Time Fourier Transform (STFT). By operating on overlapping patches, it preserves temporal structure while enhancing sensitivity to dominant low-frequency patterns.

To enable effective low-frequency learning, we first apply a low-pass filter (LPF) to the target series $Y \in \mathbb{R}^{L \times C}$ to remove high-frequency content and obtain the low-frequency supervision signal. We then compute its frequency-domain representation via the discrete Fourier transform:

$$\tilde{Y} = \text{LPF}(Y), \quad \hat{Y}_p = \text{FFT}(\tilde{Y}). \quad (3)$$

Here, \tilde{Y} denotes the filtered target series in the temporal domain, and $\hat{Y} \in \mathbb{C}^{L \times C}$ represents its frequency-domain counterpart, which is used as the supervision target in the training of PLFM. This formulation encourages the model to align with the dominant low-frequency components of the ground truth, effectively suppressing high-frequency interference and guiding the learning process toward global trends.

We then design the PLFM to predict \hat{Y} in the frequency domain. Specifically, we first process the input data X using overlapping padding with patch length P and stride S ($S < P$), and then conduct DFT on each patch and combine the transformed spectra following the previous step:

$$\begin{aligned} X_p &= \text{Patching}(X, \text{size} = P, \text{step} = S), \\ \hat{X}_p &= \text{Concat}(\text{DFT}(X_p, \text{dim} = 0)), \end{aligned} \quad (4)$$

let $N_p = \lfloor \frac{L-P+S}{S} \rfloor$, then $X_p \in \mathbb{R}^{P \times N_p \times C}$ denotes the results of X after overlapping patching and $\hat{X}_p \in \mathbb{C}^{(P \times N_p) \times C}$ will be the input of PLFM.

The detailed architecture of PLFM contains double two-layer MLPs with identical structures to model the real and imaginary

[Task]: Your task is to refine the predicted daily apply and redemption values for the next $\langle L \rangle$ days.

[History]: Recent observations for fund $\langle ID \rangle$:
date: $\langle d \rangle$ | apply: $\langle a \rangle$ | redeem: $\langle r \rangle$ | uv: $\langle u \rangle$ | yield: $\langle y \rangle$

[Prediction]: The following are model-based flow forecasts; please adjust the frequency based on supporting data:
date: $\langle pd \rangle$ | apply: $\langle pa \rangle$ | redeem: $\langle pr \rangle$ | uv: $\langle pu \rangle$ | yield: $\langle py \rangle$
apply-side: - low_freq: $\langle al \rangle \backslash n$ - high_freq: $\langle ah \rangle$
redeem-side: - low_freq: $\langle rl \rangle \backslash n$ - high_freq: $\langle rh \rangle$
Note: low_freq + high_freq = prediction

[Knowledge]: Please adjust the predictions based on:
- Higher total uv \rightarrow stronger buy-side pressure;
- Higher yield \rightarrow increased redemption potential;

Figure 4: Prompt example. $\langle \rangle$ and $\langle \rangle$ are task-specific configurations and calculated input statistics. A complete example of the prompt can be found in Appendix A

parts of spectra respectively. After that, we stack the real and imaginary predictions to form the final outputs. The process can be mathematically formulated as follows:

$$\begin{aligned} \hat{Y}_{p,\text{real}}^o &= \mathbf{W}_{\text{real}} \text{Real}(\hat{X}_p) + \mathbf{b}_{\text{real}}, \\ \hat{Y}_{p,\text{imag}}^o &= \mathbf{W}_{\text{imag}} \text{Imag}(\hat{X}_p) + \mathbf{b}_{\text{imag}}, \\ \hat{Y}_p^o &= \text{Complex}(\text{Stack}(\hat{Y}_{p,\text{real}}^o, \hat{Y}_{p,\text{imag}}^o)), \end{aligned} \quad (5)$$

where \mathbf{W}_{real} , \mathbf{b}_{real} and \mathbf{W}_{imag} , \mathbf{b}_{imag} are the learnable parameters of PLFM, and $\text{Real}(\cdot)$ and $\text{Imag}(\cdot)$ denote the operations that extract the real and imaginary parts, respectively.

Finally, PLFM takes the frequency spectra \hat{Y}_p in Equation (3) as supervised signals and learns the low-frequency dependencies through optimizing FALoss in Equation (2):

$$\mathcal{L}_{\text{FA}} = \frac{1}{L \times C} \left\| \hat{Y}_p - \hat{Y}_p^o \right\|_1. \quad (6)$$

After training, the PLFM is frozen and used during inference. Its output \hat{Y}_p^o is transformed via an Inverse Fast Fourier Transform (IFFT) into a low-frequency token Y_{low}^o , representing the predicted low-frequency component of the target sequence. Specifically, we have:

$$Y_{\text{low}}^o = \text{IFFT}(\hat{Y}_p^o). \quad (7)$$

Compared to conventional deep forecasting models that directly use temporal-domain prediction windows as supervision, where high-frequency noise may dominate and obscure meaningful patterns, our low-pass-filtered, frequency-domain supervision provides two key advantages. First, it enables the model to focus explicitly on low-frequency dependencies by removing irrelevant high-frequency components, thus improving generalization under data scarcity. Second, the resulting low-frequency signals exhibit clear and concentrated spectral peaks, allowing the model to more effectively learn global structures in the frequency domain. A visual comparison between the original signal and its low-pass filtered counterpart is illustrated in Figure 3.

Table 1: Statistics of our datasets.

Datasets	Time Frequency	Time range	Total Time Points	Prediction Target	Application Domain
FundAR	Daily	2021-01-04 to 2022-11-09	675	Apply&Redeem	Financial
Solar	Hourly	2012-04-01 to 2013-04-01	8,760	Power	Energy

3.3 Residual Learning

To complement the low-frequency forecast, we introduce a residual learner that captures the remaining high-frequency variations. Specifically, we apply a high-pass filter (HPF) to extract high-frequency components from the input and use a lightweight backbone predictor to estimate the residual signal:

$$Y_{\text{res}}^0 = f_{\text{res}}(\text{HPF}(X)), \quad (8)$$

where $Y_{\text{res}}^0 \in \mathbb{R}^{L \times C}$ is the predicted high-frequency residual token, and f_{res} denotes the residual predictor.

In this work, we adopt iTransformer [18] as the backbone for residual learning due to its lightweight architecture and strong performance on multivariate time series forecasting. During training, the predicted residual token is added to the low-frequency token Y_{low}^0 , and the combined result is aligned with the ground truth using the same FALoss. This encourages the residual learner to refine the trend-based forecast with sharp local variations while maintaining global consistency under the frequency domain.

3.4 Domain Knowledge-Injection Module via LLM Calibration

In real-world forecasting, time series often come with auxiliary signals, such as timestamps, statistical indicators, or domain-specific metrics, which are crucial for accurate prediction, especially under limited supervision. However, conventional models struggle to integrate such heterogeneous information. To overcome this, we introduce a domain knowledge-injection module that uses a LLM to semantically calibrate the initial predictions.

Specifically, we define the input to the LLM as a structured prompt \mathcal{P} that encodes the following components: (1) the low-frequency token Y_{low}^0 generated by the Low-Frequency Learner, (2) the residual token Y_{res}^0 from the Residual Learner, and (3) auxiliary variables and domain-specific knowledge relevant to the forecasting task.

The prompt is constructed in natural language form to guide the LLM in reasoning over both statistical patterns and contextual knowledge:

$$\mathcal{P} = \text{PromptBuilder}(Y_{\text{low}}^0, Y_{\text{res}}^0, A), \quad (9)$$

where $\text{PromptBuilder}(\cdot)$ represents the deterministic function for organizing model outputs and auxiliary variables into a coherent textual prompt. An illustration of the prompt structure is provided in Figure 4.

The final calibrated forecast Y^0 is generated by passing \mathcal{P} through the LLM:

$$Y^0 = \text{LLM}(\mathcal{P}). \quad (10)$$

In our implementation, we use the Qwen-3B [30] model as the backbone LLM and fine-tune it via supervised fine-tuning (SFT) using QLoRA [39] to reduce memory and compute cost. This modular

design ensures interpretability and extensibility while enabling robust semantic refinement, particularly when training data is limited or external knowledge is crucial.

4 Experiments

We comprehensively evaluate the proposed LoFT-LLM framework on two real-world time series datasets. We benchmark its performance against state-of-the-art forecasting models to demonstrate its superiority. To further validate its effectiveness, we conduct focused studies on low-frequency learning, few-shot forecasting, and ablations. These results collectively underscore LoFT-LLM's effectiveness in capturing long-term trends and integrating domain knowledge for robust, interpretable forecasting. Our codes are available at <https://github.com/yjcGitHub0/LoFT-LLM>.

4.1 Experimental Setup

Datasets. We evaluate our method on two real-world time series datasets. Summary statistics are listed in Table 1. The FundAR dataset is derived from the 2024 Alibaba Tianchi competition on fund flow forecasting [1]. We use the official raw data and retain only funds with less than 5% missing values. It provides nearly two years of daily records, including fund apply and redemption amounts, as well as auxiliary signals such as fund page views and bank certificate of deposit rates. The Solar dataset is from the 2014 Global Energy Forecasting Competition (GEFCom 2014) [9], where we focus on Region 1. It contains hourly solar power generation and meteorological indicators such as cloud cover, wind speed, and relative humidity. These datasets are representative of real-world collected time series, which are characterized by limited temporal length and rich auxiliary signals, making them well-suited for evaluating forecasting models under practical constraints.

Baselines. We evaluate our method against 12 representative baselines spanning diverse architectural families in time series forecasting, including transformer-based models (Vanilla Transformer [31], PatchTST [23], iTransformer [18], TimeXer [35]), MLP-based models (DLinear [45]), frequency decomposition-based models (FITS [40], FreTS [43], FreDF [32]), TCN-based models (TimesNet [36]), KAN-based models (TimeKAN [10]), and LLM-based models (GPT4TS [52], TimeLLM [13]). This broad coverage enables a comprehensive assessment of our framework's effectiveness and generality.

Experimental Details. We partition each dataset into training, validation, and testing sets using a 70%/10%/20% split. Given the differences in temporal resolution and sequence length, we use a look-back window of 30 time steps (one month) for the FundAR dataset and 72 time steps (three days) for the Solar dataset. Forecasting accuracy is evaluated using three standard metrics: Mean Absolute Error (MAE), Root Mean Squared Error (RMSE), and Mean Absolute Percentage Error (MAPE), with lower values indicating better performance. All experiments are conducted on a server with

Table 2: Performance comparison on the FundAR dataset. The best results are shown in bold, and the second-best results are underlined. The ‘LLM’ column indicates whether the method is based on a Large Language Model.

	LLM	1 day			2 day			3 day			4 day			5 day		
		MAE	RMSE	MAPE												
iTransformer	✗	2.299	4.227	2.313	2.352	4.453	2.757	2.280	4.129	2.181	2.278	4.133	2.225	2.276	4.103	2.123
	✗	1.859	3.525	0.993	1.893	3.561	1.255	1.907	3.583	1.274	1.919	3.599	1.399	1.903	3.579	1.309
	✗	1.231	2.720	0.615	1.212	2.706	0.656	1.158	2.693	0.670	1.159	2.694	0.673	1.214	2.724	0.671
	✗	2.115	4.052	0.823	2.092	4.011	0.828	2.183	4.166	0.863	2.224	4.258	0.842	2.236	4.268	0.872
	✗	1.021	2.417	0.824	1.031	2.484	0.975	1.073	2.570	0.963	1.135	2.637	0.999	1.138	2.643	1.009
	✗	1.524	3.071	0.736	1.550	3.116	0.716	1.625	3.220	0.743	1.608	3.198	0.723	1.551	3.102	0.732
	✗	1.123	2.584	0.689	1.207	2.728	0.741	1.246	2.808	0.760	1.230	2.783	0.752	1.261	2.833	0.789
	✗	1.270	2.790	0.766	1.213	2.668	0.804	1.210	2.682	0.759	1.314	2.848	0.792	1.243	2.750	0.769
	✗	0.982	2.443	0.609	1.027	2.530	0.612	1.040	2.580	0.624	1.053	2.626	0.631	1.068	2.654	0.622
	✗	1.076	2.507	0.599	1.202	2.718	0.618	1.216	2.713	0.640	1.213	2.735	0.679	1.164	2.673	0.602
GPT4TS	✓	1.102	2.500	0.657	1.105	2.532	0.607	1.151	2.614	0.625	1.228	2.729	0.646	1.115	2.618	0.630
TimeLLM	✓	1.136	2.535	0.639	1.163	2.588	0.640	1.171	2.614	0.674	1.227	2.688	0.691	1.247	2.720	0.663
LoFT-LLM	✓	0.661	1.758	0.433	0.671	1.786	0.450	0.700	1.851	0.487	0.703	1.878	0.500	0.770	2.087	0.569
iTransformer	LLM	6 day			7 day			8 day			9 day			10 day		
	LLM	MAE	RMSE	MAPE												
	✗	2.274	4.102	2.116	2.278	4.108	2.122	2.279	4.114	2.116	2.280	4.117	2.104	2.279	4.114	2.104
	✗	1.897	3.567	1.272	1.890	3.553	1.383	1.903	3.569	1.450	1.914	3.586	1.352	1.931	3.610	1.483
	✗	1.210	2.725	0.671	1.209	2.745	0.667	1.227	2.766	0.675	1.243	2.791	0.684	1.253	2.794	0.685
	✗	2.217	4.230	0.872	2.237	4.275	0.890	2.256	4.308	0.895	2.276	4.343	0.913	2.299	4.394	0.923
	✗	1.101	2.608	1.070	1.076	2.598	1.046	1.139	2.655	1.134	1.191	2.705	1.096	1.200	2.709	1.105
	✗	1.575	3.123	0.724	1.586	3.155	0.736	1.602	3.183	0.724	1.601	3.174	0.735	1.622	3.205	0.751
	✗	1.248	2.805	0.766	1.258	2.835	0.762	1.278	2.847	0.766	1.304	2.874	0.779	1.340	2.924	0.793
	✗	1.250	2.753	0.779	1.258	2.761	0.785	1.276	2.783	0.769	1.285	2.795	0.775	1.302	2.814	0.784
	✗	1.061	2.653	0.635	1.066	2.655	0.634	1.109	2.681	0.644	1.128	2.689	0.662	1.178	2.730	0.701
	✗	1.237	2.765	0.646	1.216	2.767	0.655	1.203	2.705	0.663	1.219	2.793	0.633	1.233	2.783	0.631
GPT4TS	✓	1.259	2.774	0.617	1.148	2.639	0.629	1.119	2.632	0.622	1.157	2.663	0.627	1.169	2.653	0.636
TimeLLM	✓	1.232	2.726	0.696	1.218	2.695	0.665	1.206	2.685	0.663	1.267	2.762	0.689	1.267	2.757	0.692
LoFT-LLM	✓	0.821	2.276	0.623	0.824	2.546	0.615	0.922	2.595	0.695	0.903	2.525	0.685	0.913	2.567	0.746

8 NVIDIA RTX 4090 GPUs (24GB VRAM each), a 128-core AMD EPYC 7513 CPU, and 503GB of RAM. Results are averaged over three independent runs to ensure robustness.

4.2 Comparative Experiments

Table 2 and Table 3 report the performance of LoFT-LLM versus 12 competitive forecasting baselines on the FundAR and Solar datasets. The results demonstrate that the proposed LoFT-LLM model consistently outperforms other baseline methods across most scenarios. Specifically, on the FundAR dataset, LoFT-LLM ranks first in 26 out of 30 evaluations and achieves an average MAE reduction of 26.53% compared to the best-performing baseline. On the Solar dataset, it ranks first in 27 out of 30 evaluations, yielding an average MAE improvement of 15.42%. This demonstrates that LoFT-LLM’s low-frequency modeling and semantic calibration effectively suppress high-frequency noise and capture stable long-term patterns in the presence of data scarcity.

We also observe that frequency-based models such as FreTS and FreDF perform well across both datasets, validating the importance of frequency decomposition in capturing underlying periodicity. Similarly, LLM-based models like GPT4TS and TimeLLM achieve competitive results in several settings, thanks to their capacity to leverage external domain knowledge. However, frequency-only models lack the ability to contextualize their predictions with auxiliary information, while LLM-only models struggle to identify

fine-grained spectral structures in noisy environments. This reflects a common challenge in real-world forecasting, where time series exhibit complex frequency dynamics (e.g., financial cycles, weather fluctuations) interspersed with abrupt or irregular patterns (e.g., policy shifts, rare weather events).

LoFT-LLM overcomes these limitations by explicitly combining frequency-aware modeling with prompt-based semantic calibration. The PLFM captures stable low-frequency patterns, while the LLM refines predictions using structured prompts that integrate low-frequency patterns, high-frequency residuals and auxiliary context. This synergy allows LoFT-LLM to simultaneously recognize global temporal structures and inject domain-specific knowledge, resulting in more robust and interpretable forecasts. The empirical results affirm the value of our hybrid design and highlight its practical advantages in real-world, data-scarce settings.

4.3 Few-Shot Forecasting

To assess the robustness of LoFT-LLM in extreme low-resource settings, we adopt few-shot configurations aligned with prior studies such as TimeLLM [13] and FSTLLM [12]. Specifically, for the FundAR dataset, only 10% of the historical records (approximately 60 time steps) are retained for training. For the Solar dataset, we use the most recent 7 days (168 time steps) as the training set. These settings simulate real-world deployment scenarios where long-term

Table 3: Performance comparison on the Solar dataset. The best results are shown in bold, and the second-best results are underlined. The 'LLM' column indicates whether the method is based on a Large Language Model.

	LLM	1 hour			2 hour			3 hour			4 hour			5 hour		
		MAE	RMSE	MAPE												
Transformer	✗	0.043	0.077	0.729	0.052	0.090	0.910	0.059	0.099	1.105	0.064	0.104	1.140	0.070	0.111	1.332
DLinear	✗	0.066	0.105	1.665	0.070	0.111	1.809	0.072	0.115	1.897	0.075	0.118	2.030	0.076	0.121	2.024
PatchTST	✗	0.043	0.071	0.905	0.051	0.085	0.992	0.056	0.092	1.214	0.057	0.096	1.161	0.060	0.100	1.129
FITS	✗	0.049	0.080	1.109	0.078	0.113	1.905	0.093	0.130	2.354	0.103	0.142	2.594	0.111	0.150	2.760
FreTS	✗	<u>0.034</u>	<u>0.067</u>	<u>0.524</u>	<u>0.040</u>	<u>0.078</u>	<u>0.603</u>	<u>0.044</u>	<u>0.087</u>	<u>0.660</u>	<u>0.047</u>	<u>0.092</u>	<u>0.633</u>	<u>0.050</u>	<u>0.096</u>	<u>0.700</u>
TimesNet	✗	0.041	0.074	0.625	0.044	0.083	0.698	0.050	0.091	0.773	0.052	0.096	0.792	0.055	0.100	0.866
iTransformer	✗	0.037	0.069	0.547	0.043	0.081	0.604	0.047	0.088	0.659	0.050	0.093	0.712	0.052	0.097	0.746
TimeXer	✗	0.044	0.072	0.984	0.050	0.084	1.079	0.054	0.091	1.048	0.056	0.096	1.040	0.057	0.100	0.960
FreDF	✗	0.043	0.076	0.688	0.048	0.088	0.756	0.053	0.097	0.830	0.057	0.103	0.906	0.059	0.107	0.930
TimeKAN	✗	0.043	0.073	0.897	0.050	0.086	0.965	0.058	0.095	1.258	0.062	0.102	1.253	0.064	0.104	1.367
GPT4TS	✓	0.052	0.089	1.058	0.053	0.096	0.953	0.056	0.100	0.947	0.058	0.105	0.939	0.060	0.108	0.987
TimeLLM	✓	0.052	0.079	0.642	0.057	0.089	0.681	0.056	0.090	0.673	0.059	0.092	0.693	0.059	0.096	0.701
LoFT-LLM	✓	0.030	0.066	0.292	0.034	0.076	0.321	0.038	0.085	0.366	0.040	0.091	0.376	0.041	0.094	0.393
	LLM	6 hour			7 hour			8 hour			9 hour			10 hour		
		MAE	RMSE	MAPE												
Transformer	✗	0.068	0.111	1.133	0.066	0.113	1.018	0.073	0.115	1.221	0.071	0.117	1.233	0.075	0.118	1.277
DLinear	✗	0.077	0.122	2.034	0.078	0.124	2.068	0.078	0.124	2.072	0.078	0.125	2.093	0.079	0.125	2.129
PatchTST	✗	0.061	0.102	1.265	0.063	0.104	1.189	0.064	0.106	1.220	0.064	0.107	1.199	0.065	0.108	1.247
FITS	✗	0.119	0.158	2.913	0.122	0.160	3.027	0.127	0.165	3.337	0.133	0.170	3.663	0.137	0.176	3.871
FreTS	✗	<u>0.051</u>	<u>0.099</u>	<u>0.733</u>	<u>0.053</u>	<u>0.102</u>	<u>0.752</u>	<u>0.054</u>	<u>0.103</u>	<u>0.792</u>	<u>0.055</u>	<u>0.104</u>	<u>0.783</u>	<u>0.056</u>	<u>0.105</u>	<u>0.794</u>
TimesNet	✗	0.057	0.104	0.857	0.059	0.104	0.930	0.059	0.106	0.944	0.060	0.107	0.906	0.062	0.109	0.923
iTransformer	✗	0.054	0.100	0.781	0.055	0.102	0.765	0.056	0.105	0.818	0.059	0.106	0.855	0.059	0.107	0.850
TimeXer	✗	0.059	0.103	0.981	0.059	0.104	0.968	0.062	0.107	0.999	0.064	0.108	1.148	0.063	0.109	1.078
FreDF	✗	0.061	0.110	0.953	0.062	0.112	0.990	0.063	0.114	1.001	0.064	0.115	0.993	0.065	0.116	1.015
TimeKAN	✗	0.064	0.108	1.268	0.066	0.108	1.372	0.066	0.109	1.250	0.068	0.111	1.307	0.069	0.113	1.599
GPT4TS	✓	0.062	0.111	1.112	0.063	0.112	1.140	0.063	0.113	0.979	0.064	0.115	1.072	0.065	0.115	1.069
TimeLLM	✓	0.061	0.098	0.780	0.064	0.106	<u>0.726</u>	0.062	0.100	<u>0.784</u>	0.061	0.099	0.796	0.063	0.101	0.825
LoFT-LLM	✓	0.043	0.098	0.409	0.044	0.100	0.420	0.045	0.102	0.428	0.046	0.104	0.522	0.047	0.104	0.526

Table 4: Few-shot forecasting results on FundAR and Solar datasets.

dataset	FundAR			Solar		
	MAE	RMSE	MAPE	MAE	RMSE	MAPE
FreTS	2.054	3.810	2.050	0.074	0.116	1.504
TimesNet	2.185	4.080	0.926	0.117	0.163	4.439
iTransformer	1.921	3.842	1.277	0.102	0.139	2.792
TimeXer	1.847	3.612	0.915	0.095	0.130	3.518
FreDF	1.739	3.556	0.901	0.096	0.138	2.122
TimeKAN	1.993	3.739	0.703	0.084	0.126	1.723
GPT4TS	1.784	3.347	0.953	0.093	0.139	3.520
TimeLLM	1.622	3.203	0.796	0.083	0.132	2.800
LoFT-LLM	0.661	1.713	0.436	0.052	0.110	0.522

historical data may be unavailable due to system cold-start, market volatility, or data privacy constraints. Such conditions pose substantial challenges for conventional deep forecasting models, which often rely heavily on extensive historical context to capture temporal dependencies and generalize to future trends.

As shown in Table 4, LoFT-LLM consistently achieves the best performance across all settings. Compared to the best-performing baseline in each task, LoFT-LLM achieves an average MAE reduction of over 40%, clearly demonstrating its effectiveness in low-data regimes. This improvement stems from the core design of our model: the PLFM effectively distills robust low-frequency trends

Table 5: Ablation results on FundAR and Solar datasets evaluating the impact of frequency learning module and LLM calibration module.

FL	LLM	FundAR			Solar		
		MAE	RMSE	MAPE	MAE	RMSE	MAPE
✗	✗	1.859	3.525	0.993	0.066	0.105	1.665
✓	✗	0.899	2.341	0.657	0.034	0.070	0.460
✗	✓	0.692	1.864	0.448	0.043	0.089	0.479
✓	✓	0.661	1.758	0.433	0.030	0.066	0.292

from limited samples by operating in the frequency domain, while the LLM-based calibration module incorporates auxiliary context and domain knowledge to semantically adjust the outputs, correcting trends and residual errors and mitigating overfitting. The synergy between frequency-aware learning and semantic reasoning allows LoFT-LLM to generalize effectively in few-shot scenarios.

4.4 Ablation Study

To assess the individual contributions of LoFT-LLM's core components, we conduct ablation experiments by systematically removing each module. As shown in Table 5, we evaluate the effect of removing (1) the frequency learning module (**FL**), which replaces the PLFM and residual learner with a simple MLP and excludes all frequency-related content from the prompt if LLM is used, and

Table 6: Experiments on the effectiveness of low-frequency learning with LoFT-LLM.

dataset	FundAR			Solar		
	MAE	RMSE	MAPE	MAE	RMSE	MAPE
FreTS	0.969	2.136	1.535	0.053	0.098	0.659
+LoFT-LLM	0.771	1.736	0.830	0.045	0.093	0.491
TimesNet	1.285	2.493	2.172	0.060	0.101	0.871
+LoFT-LLM	0.779	1.742	0.898	0.046	0.093	0.496
iTransformer	1.013	2.220	1.407	0.057	0.102	0.747
+LoFT-LLM	0.773	1.731	0.874	0.047	0.095	0.483

(2) the large language model (**LLM**), which omits the calibration stage and directly outputs the summed low- and high-frequency predictions.

The results reveal that removing either component leads to a substantial performance drop across both datasets, highlighting the effectiveness of both low-frequency modeling and semantic calibration. Interestingly, the relative impact of each module varies by dataset. On FundAR, the removal of the LLM leads to a more significant degradation than that of the frequency module, indicating that semantic calibration plays a more pivotal role in financial forecasting, where auxiliary signals like webpage uv and interest rates are crucial. In contrast, on the Solar dataset, the frequency module proves more critical, likely due to the strong periodicity and meteorological dependencies inherent in solar power generation. These findings underscore the complementary strengths of LoFT-LLM’s components and demonstrate its adaptability across diverse real-world forecasting tasks.

4.5 Analysis of Low-Frequency Learning

To evaluate the impact of our low-frequency learning strategy, we embed various mainstream forecasting models as backbone predictors into the LoFT-LLM pipeline and assess their performance on the lowest 40% of the frequency spectrum. The corresponding MAE results are shown in Table 6.

LoFT-LLM consistently lowers low-frequency MAE across all backbones, achieving an average improvement of 23% over standard training. These results highlight the effectiveness of our low-frequency design and demonstrate that LoFT-LLM serves as a general and robust enhancement pipeline for time-series forecasting.

5 Conclusion

We propose **LoFT-LLM** (Low-Frequency Time-series forecasting with Large Language Models), a unified pipeline that integrates frequency-aware learning and semantic calibration for robust time series forecasting under data scarcity. This pipeline couples a Patch Low-Frequency forecasting Module for extracting stable trend signals, a residual learner for modeling high-frequency variations, and a fine-tuned large language model for context-driven refinement through structured prompts. By jointly leveraging spectral structure and domain knowledge, LoFT-LLM achieves superior accuracy and generalization. Extensive experiments on real-world datasets confirm its effectiveness and versatility in practical forecasting scenarios.

Acknowledgements

This work was supported by the National Natural Science Foundation of China (62306085), Shenzhen College Stability Support Plan (GXWD20231130151329002), Shenzhen Science and Technology Program (KQTD20240729102207002), CCF-ALIMAMA TECH Kangaroo Fund (CCF-ALIMAMA OF 2025001).

References

- [1] FundAR dataset, alibaba tianchi competition. <https://tianchi.aliyun.com/competition/entrance/532224/information>, 2024. Accessed July 2025.
- [2] A. A. Ariyo, A. O. Adewumi, and C. K. Ayo. Stock price prediction using the arima model. In *2014 UKSim-AMSS 16th international conference on computer modelling and simulation*, pages 106–112. IEEE, 2014.
- [3] T. Brown, B. Mann, N. Ryder, M. Subbiah, J. D. Kaplan, P. Dhariwal, A. Neelakantan, P. Shyam, G. Sastry, A. Askell, et al. Language models are few-shot learners. *Advances in neural information processing systems*, 33:1877–1901, 2020.
- [4] C. Chang, W.-C. Peng, and T.-F. Chen. Llm4ts: Two-stage fine-tuning for time-series forecasting with pre-trained llms. *CoRR*, 2023.
- [5] S.-A. Chen, C.-L. Li, N. Yoder, S. O. Arik, and T. Pfister. Tsmixer: An all-mlp architecture for time series forecasting. *arXiv preprint arXiv:2303.06053*, 2023.
- [6] Y. Chen, I. Segovia-Dominguez, B. Coskunuzer, and Y. Gel. TAMP-s2GCNets: Coupling time-aware multipersistence knowledge representation with spatio-supra graph convolutional networks for time-series forecasting. In *International Conference on Learning Representations*, 2022.
- [7] V. Ekambaram, A. Jati, N. Nguyen, P. Sindhong, and J. Kalagnanam. Tsmixer: Lightweight mlp-mixer model for multivariate time series forecasting. In *Proceedings of the 29th ACM SIGKDD Conference on Knowledge Discovery and Data Mining*, pages 459–469, 2023.
- [8] H. He, Q. Zhang, S. Bai, K. Yi, and Z. Niu. Catn: cross attentive tree-aware network for multivariate time series forecasting. In *Proceedings of the AAAI Conference on Artificial Intelligence*, volume 36, pages 4030–4038, 2022.
- [9] T. Hong, P. Pinson, S. Fan, H. Zareipour, A. Troccoli, and R. J. Hyndman. Probabilistic energy forecasting: Global energy forecasting competition 2014 and beyond, 2016.
- [10] S. Huang, Z. Zhao, C. Li, and L. Bai. Timekan: Kan-based frequency decomposition learning architecture for long-term time series forecasting. *arXiv preprint arXiv:2502.06910*, 2025.
- [11] L. Jiang, B. Dai, W. Wu, and C. C. Loy. Focal frequency loss for image reconstruction and synthesis. In *Proceedings of the IEEE/CVF international conference on computer vision*, pages 13919–13929, 2021.
- [12] Y. Jiang, Y. Chen, X. Li, Q. Chao, S. Liu, and G. Cong. Fstllm: Spatio-temporal llm for few shot time series forecasting. In *Forty-second International Conference on Machine Learning*.
- [13] M. Jin, S. Wang, L. Ma, Z. Chu, J. Y. Zhang, X. Shi, P.-Y. Chen, Y. Liang, Y.-F. Li, S. Pan, et al. Time-llm: Time series forecasting by reprogramming large language models. *arXiv preprint arXiv:2310.01728*, 2023.
- [14] B. F. King. Market and industry factors in stock price behavior. *the Journal of Business*, 39(1):139–190, 1966.
- [15] T. Kojima, S. S. Gu, M. Reid, Y. Matsuo, and Y. Iwasawa. Large language models are zero-shot reasoners. *Advances in neural information processing systems*, 35:22199–22213, 2022.
- [16] G. Lai, W.-C. Chang, Y. Yang, and H. Liu. Modeling long-and short-term temporal patterns with deep neural networks. In *The 41st international ACM SIGIR conference on research & development in information retrieval*, pages 95–104, 2018.
- [17] C. Liu, H. Miao, Q. Xu, S. Zhou, C. Long, Y. Zhao, Z. Li, and R. Zhao. Efficient multivariate time series forecasting via calibrated language models with privileged knowledge distillation. *arXiv preprint arXiv:2505.02138*, 2025.
- [18] Y. Liu, T. Hu, H. Zhang, H. Wu, S. Wang, L. Ma, and M. Long. itransformer: Inverted transformers are effective for time series forecasting. *arXiv preprint arXiv:2310.06625*, 2023.
- [19] Y. Liu, G. Qin, X. Huang, J. Wang, and M. Long. Autotimes: Autoregressive time series forecasters via large language models. *Advances in Neural Information Processing Systems*, 37:122154–122184, 2024.
- [20] Y. Liu, H. Wu, J. Wang, and M. Long. Non-stationary transformers: Exploring the stationarity in time series forecasting. *Advances in neural information processing systems*, 35:9881–9893, 2022.
- [21] E. N. Lorenz. *Empirical orthogonal functions and statistical weather prediction*, volume 1. Massachusetts Institute of Technology, Department of Meteorology Cambridge, 1956.
- [22] S. Min, X. Lyu, A. Holtzman, M. Artetxe, M. Lewis, H. Hajishirzi, and L. Zettlemoyer. Rethinking the role of demonstrations: What makes in-context learning work? *arXiv preprint arXiv:2202.12837*, 2022.
- [23] Y. Nie, N. H. Nguyen, P. Sindhong, and J. Kalagnanam. A time series is worth 64 words: Long-term forecasting with transformers. In *International Conference on*

Learning Representations, 2023.

[24] Y. Nie, N. H. Nguyen, P. Sinthong, and J. Kalagnanam. A time series is worth 64 words: Long-term forecasting with transformers. *arXiv preprint arXiv:2211.14730*, 2022.

[25] M. Plancherel and M. Leffler. Contribution à l'étude de la représentation d'une fonction arbitraire par des intégrales définies. *Rendiconti del Circolo Matematico di Palermo (1884-1940)*, 30(1):289–335, 1910.

[26] N. Rahaman, A. Baratin, D. Arpit, F. Draxler, M. Lin, F. Hamprecht, Y. Bengio, and A. Courville. On the spectral bias of neural networks. In *International conference on machine learning*, pages 5301–5310. PMLR, 2019.

[27] D. Salinas, V. Flunkert, J. Gasthaus, and T. Januschowski. Deepar: Probabilistic forecasting with autoregressive recurrent networks. *International journal of forecasting*, 36(3):1181–1191, 2020.

[28] X. Shi, S. Wang, Y. Nie, D. Li, Z. Ye, Q. Wen, and M. Jin. Time-moe: Billion-scale time series foundation models with mixture of experts. *arXiv preprint arXiv:2409.16040*, 2024.

[29] X. Song, Q. Wen, Y. Li, and L. Sun. Robust time series dissimilarity measure for outlier detection and periodicity detection. In *Proceedings of the 31st ACM International Conference on Information & Knowledge Management*, pages 4510–4514, 2022.

[30] Q. Team. Owen3 technical report, 2025.

[31] A. Vaswani, N. Shazeer, N. Parmar, J. Uszkoreit, L. Jones, A. N. Gomez, Ł. Kaiser, and I. Polosukhin. Attention is all you need. *Advances in neural information processing systems*, 30, 2017.

[32] H. Wang, L. Pan, Z. Chen, D. Yang, S. Zhang, Y. Yang, X. Liu, H. Li, and D. Tao. Fredf: Learning to forecast in the frequency domain. *arXiv preprint arXiv:2402.02399*, 2024.

[33] W. Wang, J. Wang, C. Chen, J. Jiao, Y. Cai, S. Song, and J. Li. Fremim: Fourier transform meets masked image modeling for medical image segmentation. In *Proceedings of the IEEE/CVF Winter Conference on Applications of Computer Vision*, pages 7860–7870, 2024.

[34] X. Wang, M. Feng, J. Qiu, J. Gu, and J. Zhao. From news to forecast: Integrating event analysis in lilm-based time series forecasting with reflection. *Advances in Neural Information Processing Systems*, 37:58118–58153, 2024.

[35] Y. Wang, H. Wu, J. Dong, G. Qin, H. Zhang, Y. Liu, Y. Qiu, J. Wang, and M. Long. Timexer: Empowering transformers for time series forecasting with exogenous variables. *Advances in Neural Information Processing Systems*, 37:469–498, 2024.

[36] H. Wu, T. Hu, Y. Liu, H. Zhou, J. Wang, and M. Long. Timesnet: Temporal 2d-variation modeling for general time series analysis. In *The eleventh international conference on learning representations*, 2022.

[37] H. Wu, J. Xu, J. Wang, and M. Long. Autoformer: Decomposition transformers with auto-correlation for long-term series forecasting. *Advances in neural information processing systems*, 34:22419–22430, 2021.

[38] J. Xie, W. Li, X. Zhan, Z. Liu, Y. S. Ong, and C. C. Loy. Masked frequency modeling for self-supervised visual pre-training. *arXiv preprint arXiv:2206.07706*, 2022.

[39] Y. Xu, L. Xie, X. Gu, X. Chen, H. Chang, H. Zhang, Z. Chen, X. Zhang, and Q. Tian. Qa-lora: Quantization-aware low-rank adaptation of large language models. *arXiv preprint arXiv:2309.14717*, 2023.

[40] Z. Xu, A. Zeng, and Q. Xu. Fits: Modeling time series with 10k parameters. *arXiv preprint arXiv:2307.03756*, 2023.

[41] Z.-Q. J. Xu, Y. Zhang, T. Luo, Y. Xiao, and Z. Ma. Frequency principle: Fourier analysis sheds light on deep neural networks. *arXiv preprint arXiv:1901.06523*, 2019.

[42] K. Yi, Q. Zhang, W. Fan, S. Wang, P. Wang, H. He, N. An, D. Lian, L. Cao, and Z. Niu. Frequency-domain mlps are more effective learners in time series forecasting. In A. Oh, T. Naumann, A. Globerson, K. Saenko, M. Hardt, and S. Levine, editors, *Advances in neural information processing systems*, volume 36, pages 76656–76679. Curran Associates, Inc., 2023.

[43] K. Yi, Q. Zhang, W. Fan, S. Wang, P. Wang, H. He, N. An, D. Lian, L. Cao, and Z. Niu. Frequency-domain mlps are more effective learners in time series forecasting. *Advances in Neural Information Processing Systems*, 36:76656–76679, 2023.

[44] T. Yucelen and W. M. Haddad. Low-frequency learning and fast adaptation in model reference adaptive control. *IEEE Transactions on Automatic Control*, 58(4):1080–1085, 2012.

[45] A. Zeng, M. Chen, L. Zhang, and Q. Xu. Are transformers effective for time series forecasting? In *Proceedings of the AAAI conference on artificial intelligence*, volume 37, pages 11121–11128, 2023.

[46] T. Zhang, Y. Zhang, W. Cao, J. Bian, X. Yi, S. Zheng, and J. Li. Less is more: Fast multivariate time series forecasting with light sampling-oriented mlp structures. *arXiv preprint arXiv:2207.01186*, 2022.

[47] Z. Zhao, W. S. Lee, and D. Hsu. Large language models as commonsense knowledge for large-scale task planning. *Advances in neural information processing systems*, 36:31967–31987, 2023.

[48] Y. Zheng, X. Yi, M. Li, R. Li, Z. Shan, E. Chang, and T. Li. Forecasting fine-grained air quality based on big data. In *Proceedings of the 21th ACM SIGKDD international conference on knowledge discovery and data mining*, pages 2267–2276, 2015.

[49] H. Zhou, S. Zhang, J. Peng, S. Zhang, J. Li, H. Xiong, and W. Zhang. Informer: Beyond efficient transformer for long sequence time-series forecasting. In *Proceedings of the AAAI conference on artificial intelligence*, volume 35, pages 11106–11115, 2021.

[50] T. Zhou, Z. Ma, Q. Wen, L. Sun, T. Yao, W. Yin, R. Jin, et al. Film: Frequency improved legendre memory model for long-term time series forecasting. *Advances in neural information processing systems*, 35:12677–12690, 2022.

[51] T. Zhou, Z. Ma, Q. Wen, X. Wang, L. Sun, and R. Jin. Fedformer: Frequency enhanced decomposed transformer for long-term series forecasting. In *International conference on machine learning*, pages 27268–27286. PMLR, 2022.

[52] T. Zhou, P. Niu, L. Sun, R. Jin, et al. One fits all: Power general time series analysis by pretrained lm. *Advances in neural information processing systems*, 36:43322–43355, 2023.

A Prompt Design for LLM Refinement

A.1 FundAR Prompt

This section provides a representative example of the prompt used for LoFT-LLM calibration in the FundAR dataset. As shown in Figure 5, the prompt is carefully structured to present the LLM with both model-derived forecasting signals and relevant auxiliary variables. This design enables the LLM to semantically reason over time-aligned patterns, adjust for systematic biases, and incorporate domain-specific knowledge that is otherwise difficult to encode through conventional parametric models.

```

### Role: Financial Sequence Analyst
You are a quantitative analyst focusing on fund capital flow modeling.
Your task is to **refine the predicted daily subscription ('apply_amt') and redemption ('redeem_amt') values for the next 2 calendar days** for fund '2', leveraging historical transaction behavior, macroeconomic indicators, and behavioral signals.

### Feature Description
- 'apply_amt': Net fund subscriptions (actual values).
- 'redeem_amt': Net fund redemptions (actual values).
- 'yield': 1-year interbank CD yield (%), reflecting opportunity cost.
- 'is_trade': 1 = trading day; 0 = non-trading day.
- 'is_month_end': 1 = last trading day of the month, often tied to institutional behavior.
- 'Total UV': Total user views on fund-related content (attention measure).
- 'Selected-fund preference ratio': Buy-side intent signal = 'uv_fundopt / total_uv'.

### Historical Data Context: Past 30 Calendar Days
Recent observations for fund '2':
- 20220704 | apply: 18.092, redeem: 15.431, yield: 0.023200, Total UV: 11931860992, Selected-fund preference ratio: 0.35, month_end: 0, is_trade: 1
- 20220705 | apply: 11.392, redeem: 10.670, yield: 0.023350, Total UV: 7782804992, Selected-fund preference ratio: 0.40, month_end: 0, is_trade: 1
- 20220706 | apply: 7.685, redeem: 13.551, yield: 0.023100, Total UV: 8805384192, Selected-fund preference ratio: 0.41, month_end: 0, is_trade: 1
.....

### Prediction Window: Next 2 Calendar Days
The following are model-based flow forecasts; please adjust the frequency based on supporting data:
- 20220802 | predicted apply: 11.296, predicted redeem: 7.671, yield: 0.019400, Total UV: 7307098624, Selected-fund preference ratio: 0.37, month_end: 0, is_trade: 1
- 20220803 | predicted apply: 11.261, predicted redeem: 7.753, yield: 0.019400, Total UV: 7014362112, Selected-fund preference ratio: 0.38, month_end: 0, is_trade: 1

### Frequency Component Reference
- 'predicted_apply = low_freq + high_freq'
- 'predicted_redeem = low_freq + high_freq'

Apply-side:
- low_freq: [10.356, 10.179]
- high_freq: [0.940, 1.082]

Redeem-side:
- low_freq: [7.029, 7.000]
- high_freq: [0.642, 0.753]

### Instructions
Please adjust the model-generated 'apply_amt' and 'redeem_amt' predictions based on:
- Investor intent signals (UVs and preference ratio);
- Yield as an indicator of fund attractiveness;
- Structural seasonality (month-end);
- Historical trends and financial intuition.

Treat the provided forecast as a **base estimate** requiring refinement. Pay attention to:
- Higher **preference ratio** → stronger buy-side pressure.
- Higher **yield** → increased redemption potential.

### Output Format (Strict)
Return **two lists of 2 float values**, representing:
1. Refined 'apply_amt' predictions
2. Refined 'redeem_amt' predictions

No explanations, comments, or variable names.

Example:
[float, float]
[float, float]

Task Instruction  Semantic Information  Historical Sequence  Future Feature & Low-Frequency Token & Residual Token  Domain-Specific Knowledge

```

Figure 5: An example of the input prompt used for LLM calibration on the FundAR dataset.

A.2 Solar Prompt

In this section, we present a detailed evaluation prompt example used by LSTLLM to provide predictions on Solar dataset as in Figure 6.

```
You are an expert assistant helping improve hourly solar-power forecasts. The target variable POWER is the site's irradiance per unit area, already normalised to the range [0, 1] (W m-2 divided by 1000). We need corrections for the next 2 hours.

### Feature Descriptions:
SSRD_eff (J m-2 h-1), Cloud_opt (optical depth index), Wind_speed (m s-1), RH_cloud (%), SSRD_delta (J m-2 change), Suppression_score (composite cloud/ humidity penalty).

### Historical observations (1 h resolution)
- 20130116 19:00 | POWER:0.0001, SSRD_eff:19655146.0, Cloud_opt:9.74, Wind_speed:1.60, RH_cloud:15.7, SSRD_delta:0.0, Suppression:43.61
- 20130116 20:00 | POWER:0.0218, SSRD_eff:20992478.0, Cloud_opt:8.11, Wind_speed:1.37, RH_cloud:11.2, SSRD_delta:134128.0, Suppression:43.34
- 20130116 21:00 | POWER:0.1213, SSRD_eff:16029467.0, Cloud_opt:4.05, Wind_speed:1.07, RH_cloud:28.4, SSRD_delta:781248.0, Suppression:39.92
.....

### Preliminary forecast (next 2 h)
The following are model-based power forecasts; please adjust the frequency based on supporting data:
- 20130118 01:00 | Pred_POWER:0.7400, SSRD_eff:218045.4, Cloud_opt:202.92, Wind_speed:8.59, RH_cloud:20.8, SSRD_delta:0.0, Suppression:21.28
- 20130118 02:00 | Pred_POWER:0.7129, SSRD_eff:1844256.8, Cloud_opt:26.57, Wind_speed:7.55, RH_cloud:14.6, SSRD_delta:1441912.0, Suppression:13.29

### Frequency Component Reference
- `predicted_power = low_freq + high_freq`
- `low_freq`: trend component — [0.674, 0.789]
- `high_freq`: fluctuation component — [0.065, -0.076]

### Your Task
You must **adjust** the predicted POWER values considering:
1. **Deep-shade block** 09 : 00 – 20 : 00 local time → POWER = 0.
2. **Twilight taper** 08 → 09 must glide down to zero; 20 → 22 must rise smoothly from zero.
3. **Main drivers**
  • Positive: one-hour GHI (SSRD_diff / Δt) if > 0 (p≈+0.86); 2 m air-temperature (p≈+0.54).
  • Negative: RH_cloud (p≈-0.55), Cloud_opt & Suppression_score (≈-0.12 ~ -0.23).
  • Wind_Speed now shows only a weak positive link (p≈+0.11).
4. **Adjustment logic**
  • Raise POWER when GHI rises **and** cloud / suppression signals are low.
  • Cut or zero spikes when Cloud_opt or Suppression_score is high, or RH_cloud > 80 %.
5. **Continuity** |ΔPOWER| ≤ 0.33 unless a matching jump in GHI justifies it.
6. **Bounds** Clip all outputs to [0, 1] and keep the daylight profile above.

### Output Format (Strict)
Return the corrected POWER values (length = 2), all within [0, 1].
No explanations, comments, or variable names.
Example:
[float, float]
```

Task Instruction Semantic Information Historical Sequence Future Feature & Low-Frequency Token & Residual Token Domain-Specific Knowledge

Figure 6: An example of the input prompt used for LLM calibration on the Solar dataset.

A.3 Prompt Construction and Inference Execution

To ensure consistent structure, semantic clarity, and domain relevance across different datasets, we employed ChatGPT-4o to assist in the generation of prompt descriptions and templates. This helped standardize prompt patterns while maintaining flexibility to accommodate various forecasting contexts. Examples are illustrated in Figure 5 and Figure 6.

To further constrain the LLM's output behavior and improve numerical accuracy, we fine-tune it using a prompt-to-sequence alignment task. Specifically, for each training instance, we concatenate the historical prompt with a ground-truth target sequence formatted as a numeric list (e.g., [2.523, 1.776]). This supervised fine-tuning guides the model to generate outputs that are not only structurally consistent but also closely aligned with actual future values.

At inference time, the fine-tuned LLM receives a prompt and directly outputs the calibrated forecast in the same numeric list format (e.g., [2.481, 1.783]), representing the refined values for each time step in the prediction horizon. We then parse and convert this output into floating-point arrays, which are used as the final prediction results of our model.

B Theoretical Insights on FALoss

This section includes more explanation of FALoss and MSE from the perspective of energy and also provides corresponding theoretical insights.

Theorem 1. According to Parseval-Plancherel identity [25], the energy of the raw signal in the temporal domain is equal to the energy of its representation in the frequency domain. It can be formulated as follows:

$$\sum_{n=0}^{N-1} |x_n|^2 = \frac{1}{N} \sum_{k=0}^{N-1} |\hat{x}_k|^2, \quad (11)$$

where x_n denotes the data point, \hat{x}_k represents the k -th Fourier coefficient of the raw signal.

PROOF. Let x_n^* represents the complex conjugate of x_n . According to the conjugation of IDFT, $x_n^* = \frac{1}{N} \sum_{k=0}^{N-1} \hat{x}_k^* \cdot e^{-\frac{i2\pi}{N} kn}$, then

$$\begin{aligned} \sum_{n=0}^{N-1} |x_n|^2 &= \sum_{n=0}^{N-1} x_n \cdot x_n^* \\ &= \sum_{n=0}^{N-1} x_n \left[\frac{1}{N} \sum_{k=0}^{N-1} \hat{x}_k^* \cdot e^{-\frac{i2\pi}{N} kn} \right] \\ &= \sum_{k=0}^{N-1} \hat{x}_k^* \cdot \frac{1}{N} \sum_{n=0}^{N-1} x_n \cdot e^{-\frac{i2\pi}{N} kn} \\ &= \frac{1}{N} \sum_{k=0}^{N-1} \hat{x}_k^* \hat{x}_k \\ &= \frac{1}{N} \sum_{k=0}^{N-1} |\hat{x}_k|^2. \end{aligned}$$

Proved. \square

According to eq. (11), the energy of a time series in the temporal domain is equal to the energy of its representation in the frequency domain. From the energy perspective, conventional loss functions in the temporal domain, such as MSE, allocate energy to every time step and leverage point-wise alignment, which imposes strains on global alignment. Compared with MSE and other training metrics in the temporal domain, FALoss distributes energy to every Fourier frequency component obtained from the global data and aligns the corresponding frequency components, subsequently promoting global alignment.

Theorem 2. Suppose that $f(t)$ represents prediction window and $g(t)$ represents the model output, then the MAE between $f(t)$ and $g(t)$ can be reduced by optimizing the differences between the corresponding frequency components in the spectrum. This can be given by:

$$\text{MAE}(f(t), g(t)) \leq \sum_{k=0}^{N-1} |\hat{x}_k - \hat{y}_k|, \quad (12)$$

where \hat{x}_k and \hat{y}_k represent the k -th Fourier coefficient of $f(t)$ and $g(t)$ respectively, and N is the length of the raw signal.

PROOF. Given $f(t) = [x_0, x_1, \dots, x_{N-1}]$ and $g(t) = [y_0, y_1, \dots, y_{N-1}]$, let us consider the inversed Discrete Fourier Transform (IDFT) on $f(t)$ and $g(t)$, then

$$\begin{aligned} x_n &= \sum_{k=0}^{N-1} \hat{x}_k \cdot e^{\frac{i2\pi}{N} kn}, \\ y_n &= \sum_{k=0}^{N-1} \hat{y}_k \cdot e^{\frac{i2\pi}{N} kn}. \end{aligned}$$

We can obtain

$$\begin{aligned}
 \text{MAE}(f(t), g(t)) &= \frac{1}{N} \sum_{n=0}^{N-1} |x_n - y_n| \\
 &= \frac{1}{N} \sum_{n=0}^{N-1} \left| \sum_{k=0}^{N-1} \hat{x}_k \cdot e^{\frac{i2\pi}{N} kn} - \sum_{k=0}^{N-1} \hat{y}_k \cdot e^{\frac{i2\pi}{N} kn} \right| \\
 &= \frac{1}{N} \sum_{n=0}^{N-1} \left| \sum_{k=0}^{N-1} (\hat{x}_k - \hat{y}_k) \cdot e^{\frac{i2\pi}{N} kn} \right|.
 \end{aligned}$$

According to the absolute value inequality $|\sum a_i| \leq \sum |a_i|$, then

$$\begin{aligned}
 \text{MAE}(f(t), g(t)) &= \frac{1}{N} \sum_{n=0}^{N-1} \left| \sum_{k=0}^{N-1} (\hat{x}_k - \hat{y}_k) \cdot e^{\frac{i2\pi}{N} kn} \right| \\
 &\leq \sum_{n=0}^{N-1} \sum_{k=0}^{N-1} |\hat{x}_k - \hat{y}_k| \cdot \left| e^{\frac{i2\pi}{N} kn} \right|.
 \end{aligned}$$

Considering $\left| e^{\frac{i2\pi}{N} kn} \right| = 1$, therefore

$$\text{MAE}(f(t), g(t)) \leq \sum_{k=0}^{N-1} |\hat{x}_k - \hat{y}_k|.$$

Proved. \square

eq. (12) illustrates that optimizing \mathcal{L}_{FA} can reduce the upper bound of MAE between the ground truth and model output in the temporal domain, further guaranteeing the effectiveness of \mathcal{L}_{FA} .

C Details on the standard deviation

Standard deviation measures how much data deviates from the mean, reflecting the variability or consistency of a dataset: larger values indicate greater dispersion, while smaller values suggest tighter clustering around the mean. In our experiments, all results are averaged over three independent runs. Table 7 reports the average standard deviation of the experimental results on the two datasets.

Table 7: Experiments on the effectiveness of low-frequency learning with LoFT-LLM.

stdev	Financial			Solar		
	MAE	RMSE	MAPE	MAE	RMSE	MAPE
Transformer	0.0233	0.0276	0.1697	0.0037	0.0019	0.1867
DLinear	0.0115	0.0165	0.0914	0.0011	0.0012	0.0629
PatchTST	0.0175	0.0241	0.0206	0.0017	0.0007	0.0912
FITS	0.0426	0.0876	0.0131	0.0151	0.0144	0.3965
FreTS	0.0596	0.0600	0.1010	0.0004	0.0004	0.0306
TimesNet	0.0391	0.0695	0.0264	0.0016	0.0020	0.0845
iTransformer	0.0311	0.0561	0.0214	0.0011	0.0007	0.0552
TimeXer	0.0359	0.0514	0.0276	0.0014	0.0004	0.1085
GPT4TS	0.0601	0.0638	0.0208	0.0010	0.0012	0.0786
TimeLLM	0.0278	0.6663	0.0179	0.0071	0.0127	0.1577
FreDF	0.0219	0.0237	0.0139	0.0007	0.0010	0.0284
TimeKAN	0.0657	0.0749	0.0449	0.0018	0.0018	0.1138
TS-LFL	0.0065	0.0216	0.0138	0.0003	0.0005	0.0151
FALoss+LLM	0.0192	0.1259	0.0195	0.0003	0.0007	0.0028

D Visualizing PLFM's Frequency-Domain Predictions

We visualize the forecasting spectrum of PLFM, as shown in Figure 7, to further demonstrate that PLFM can discover clear dependencies in the frequency domain. It can be observed that the outputs of PLFM fit well in the frequency domain, further highlighting its effectiveness in capturing low-frequency signals.

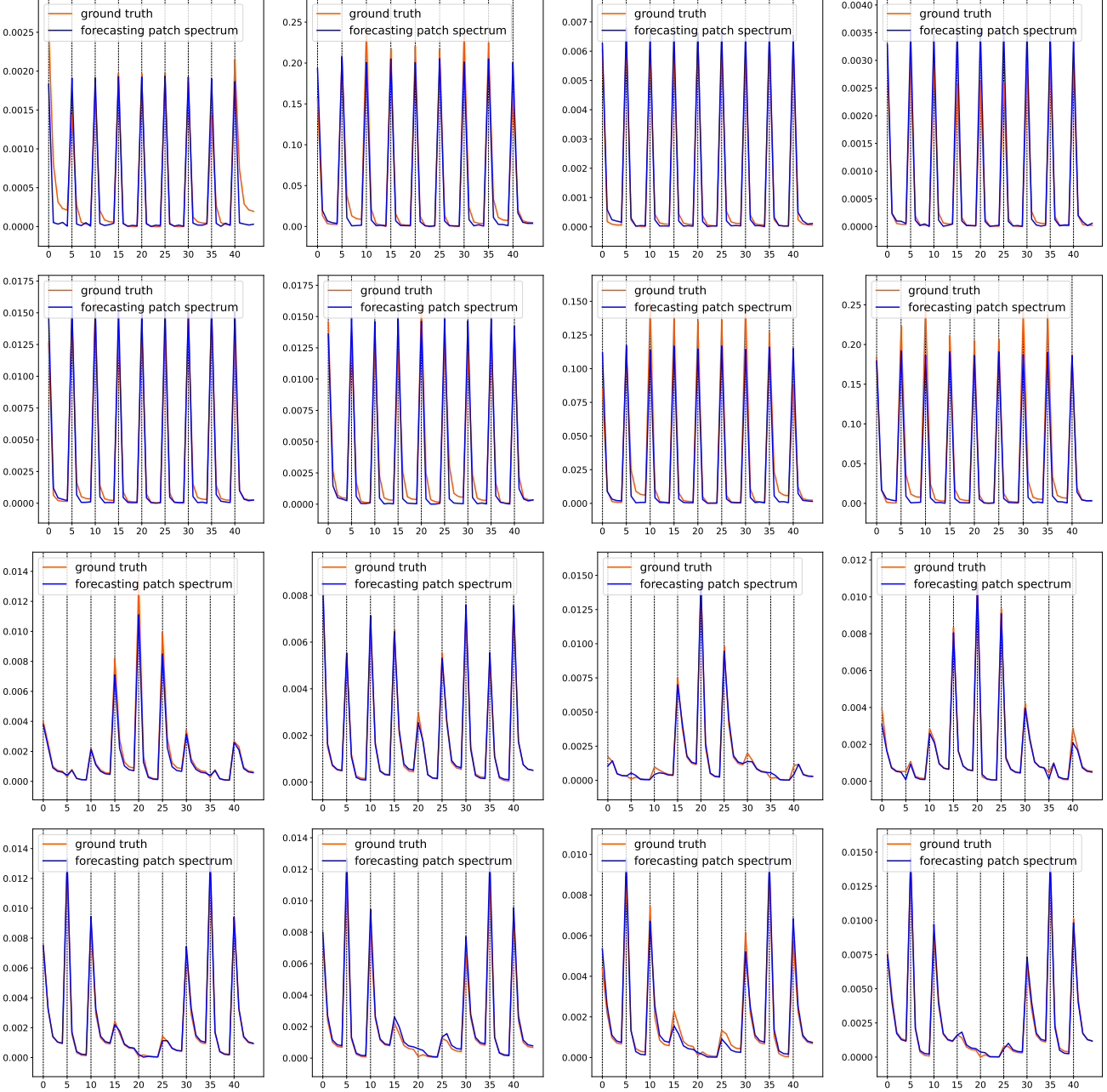


Figure 7: Visualization of forecasting spectrum of PLFM on the FundAR and Solar datasets.

E Analysis of patch length

To examine how different patch lengths in the Patch Low-Frequency Forecasting Module affect the final performance, we conducted experiments with varying patch length configurations. The results are presented in the Table 8.

Table 8: The performance of LoFT-LLM on the FundAR dataset under different patch lengths.

patchlen	1 day			2 day			3 day			4 day			5 day		
	MAE	RMSE	MAPE	MAE	RMSE	MAPE									
8	0.662	1.745	0.443	0.664	1.795	0.457	0.686	1.846	0.472	0.700	1.889	0.496	0.728	1.940	0.573
10	0.660	1.749	0.427	0.663	1.779	0.449	0.688	1.846	0.488	0.691	1.860	0.489	0.732	1.945	0.579
12	0.655	1.726	0.420	0.666	1.769	0.463	0.690	1.867	0.480	0.686	1.859	0.515	0.736	1.976	0.567
14	0.657	1.756	0.432	0.663	1.777	0.455	0.692	1.834	0.472	0.697	1.872	0.488	0.732	1.950	0.574
16	0.661	1.749	0.427	0.669	1.782	0.469	0.684	1.834	0.468	0.691	1.865	0.517	0.728	1.957	0.558
patchlen	6 day			7 day			8 day			9 day			10 day		
	MAE	RMSE	MAPE	MAE	RMSE	MAPE									
8	0.751	2.000	0.648	0.763	2.042	0.589	0.795	2.105	0.658	0.784	2.087	0.628	0.785	2.094	0.623
10	0.757	2.016	0.622	0.758	2.058	0.586	0.792	2.072	0.655	0.778	2.076	0.604	0.783	2.079	0.620
12	0.757	2.015	0.637	0.756	2.024	0.596	0.783	2.059	0.654	0.773	2.051	0.610	0.778	2.069	0.637
14	0.753	2.013	0.614	0.760	2.034	0.575	0.782	2.060	0.638	0.786	2.084	0.638	0.776	2.064	0.629
16	0.750	1.993	0.635	0.756	2.014	0.587	0.797	2.103	0.662	0.782	2.095	0.614	0.780	2.089	0.628